Spatial gene expression changes in the mouse heart after base-targeted irradiation

Walls, G. M., Ghita, M., Queen, R., Edgar, K. S., Gill, E. K., Kuburas, R., Grieve, D. J., Watson, C. J., McWilliam, A., Van Herk, M., Williams, K. J., Cole, A. J., Jain, S., & Butterworth, K. T. (2023). Spatial gene expression changes in the mouse heart after base-targeted irradiation. *International Journal of Radiation Oncology - Biology - Physics*, *115*(2), 453-463. https://doi.org/10.1016/j.ijrobp.2022.08.031

Published in:
International Journal of Radiation Oncology - Biology - Physics

Document Version:
Publisher's PDF, also known as Version of record

INTERNATIONAL JOURNAL OF
RADIATION ONCOLOGY • BIOLOGY • PHYSICS
www.redjournal.org

BIOLOGY CONTRIBUTION

Spatial Gene Expression Changes in the Mouse Heart After Base-Targeted Irradiation

Gerard M. Walls, FRCR,[*,†] Mihaela Ghita, PhD,[*] Rachel Queen, PhD,[‡] Kevin S. Edgar, PhD,[§] Eleanor K. Gill, PhD,[§,‖] Refik Kuburas, PhD,[*] David J. Grieve, PhD,[§] Chris J. Watson, PhD,[§] Alan McWilliam, PhD,[¶,#] Marcel Van Herk, PhD,[¶,#] Kaye J. Williams, PhD,[**] Aidan J. Cole, FRCR, PhD,[*,†] Suneil Jain, FRCR, PhD,[*,†] and Karl T. Butterworth, PhD[*]

[*]*Patrick G Johnston Centre for Cancer Research, Queen's University Belfast, Northern Ireland;* [†]*Cancer Centre Belfast City Hospital, Belfast Health & Social Care Trust, Belfast, Northern Ireland;* [‡]*Biosciences Institute, Faculty of Medical Sciences, Newcastle University, Newcastle-upon-Tyne, England;* [§]*Wellcome-Wolfson Institute for Experimental Medicine, Queen's University Belfast, Belfast, Northern Ireland;* [‖]*Department of Physiology, Anatomy and Genetics, University of Oxford, Oxford, England;* [¶]*Division of Cancer Sciences, University of Manchester, Oglesby Building, Manchester, England;* [#]*Department of Radiation Therapy Related Research, The Christie Foundation Trust, Manchester, England; and* [**]*Division of Pharmacy and Optometry, School of Health Science, Faculty of Biology Medicine and Health, University of Manchester, Manchester, England*

Received Mar 30, 2022; Accepted for publication Aug 5, 2022

Purpose: Radiation cardiotoxicity (RC) is a clinically significant adverse effect of treatment for patients with thoracic malignancies. Clinical studies in lung cancer have indicated that heart substructures are not uniformly radiosensitive, and that dose to the heart base drives RC. In this study, we aimed to characterize late changes in gene expression using spatial transcriptomics in a mouse model of base regional radiosensitivity.

Methods and Materials: An aged female C57BL/6 mouse was irradiated with 16 Gy delivered to the cranial third of the heart using a 6 × 9 mm parallel opposed beam geometry on a small animal radiation research platform, and a second mouse was sham-irradiated. After echocardiography, whole hearts were collected at 30 weeks for spatial transcriptomic analysis to map gene expression changes occurring in different regions of the partially irradiated heart. Cardiac regions were manually annotated on the capture slides and the gene expression profiles compared across different regions.

Results: Ejection fraction was reduced at 30 weeks after a 16 Gy irradiation to the heart base, compared with the sham-irradiated controls. There were markedly more significant gene expression changes within the irradiated regions compared with nonirradiated regions. Variation was observed in the transcriptomic effects of radiation on different cardiac base structures (eg, between the right atrium [n = 86 dysregulated genes], left atrium [n = 96 dysregulated genes], and the vasculature [n = 129 dysregulated genes]). Disrupted biological processes spanned extracellular matrix as well as circulatory, neuronal, and contractility activities.

Corresponding author: Gerard Walls; E-mail: g.walls@qub.ac.uk

This work was performed within the Irish Clinical Academic Training (ICAT) Programme, supported by the Wellcome Trust and the Health Research Board (Grant Number 203930/B/16/Z), the Health Service Executive National Doctors Training and Planning and the Health and Social Care, Research and Development Division, Northern Ireland (GW, AC, SJ, KB). MG, RF and KB are supported by the Medical Research Council (MR/V009605/1). EG, KE, DG and CW are supported by the British Heart Foundation. RQ is supported by the Spartan Programme. AM, MV and KW are supported by the Cancer Research UK RadNet Manchester programme [C1994/A28701], and AM and MV also receive support from the NIHR Manchester Biomedical Research Centre.

Disclosures: none.

The data are not available for sharing at the time of publication.

Acknowledgments—The authors wish to thank Gordon McGregor and Lynne Overman for their technical input during the study and Steve Lisgo for his role in planning this research.

Supplementary material associated with this article can be found in the online version at doi:10.1016/j.ijrobp.2022.08.031.

Int J Radiation Oncol Biol Phys, Vol. 115, No. 2, pp. 453–463, 2023

https://doi.org/10.1016/j.ijrobp.2022.08.031

Conclusions: This is the first study to report spatially resolved gene expression changes in irradiated tissues. Examination of the regional radiation response in the heart can help to further our understanding of the cardiac base's radiosensitivity and support the development of actionable targets for pharmacologic intervention and biologically relevant dose constraints.

Introduction

Radiation cardiotoxicity (RC) is as an important sequela of treatment for patients with lung, esophagus, breast, and mediastinal malignancies, despite recent advances in radiation therapy technology.[1-4] RC is manifested as ischemia, arrhythmia, heart failure, valvulopathy, or pericardial disease in the months or years posttreatment.[5,6] The affected underlying cardiac tissues are highly interdependent in their orchestration of the heart's overall function, maintaining systemic blood pressure.[7-9] Given this complexity, it is likely that radiation-related pathologies of the heart in select substructures may affect other regions of the heart through mechanical aberration or downstream biological effects. For example, ischemic vascular events can cause arrhythmias[8] and pericardial disease,[10] and valvular[11] and pericardial problems[12] can precipitate muscular pump failure (ie, heart failure).

RC is primarily determined by the relative anatomic relationship of thoracic tumors and the heart. For example, left-sided tangential breast fields are associated with premature left anterior descending coronary artery disease, and mediastinal field geometries for lymphoma are associated with valvular stenosis or regurgitation.[13] Modern radiation therapy planning and conformal delivery techniques have significantly reduced the probability of normal tissue complication,[14] yet recent evidence indicates that the heart remains a critical organ at risk that displays regional radiosensitivity characteristics, with the heart base being particularly important.[15-17] The base of the heart includes the proximal portion of "serial" organs such as the coronary arteries and the cardiac conduction system, as well as "parallel" structures such as the atrial myocardium. It is likely that there is variation in the radiation response of these substructures, governed by their underlying nonuniform alpha/beta ratios.[18]

We have previously demonstrated regional radiosensitivity in the heart in a preclinical model of RC by targeting the base of the heart.[19] In this study, we use the same partial heart irradiation model to characterize the late-occurring gene expression (GE) changes in different heart regions using spatial transcriptomics. This approach provides a high-resolution presentation of the spatial gene expression landscape to better understand radiobiological response after targeted irradiation. These data can help to directly inform the development of preventative strategies such as pharmacologic interventions and biologically derived substructure dose constraints to reduce the probability of adverse reactions in the heart.

Methods and Materials

Animals

Female C57BL6J mice aged 9 months (Charles River Laboratories, Oxford, UK) were housed under controlled conditions (12-hour light-dark cycle, 21°C) in standard caging with 3 to 5 littermates and received a standard diet (Teklad, Envigo, UK) with water ad libitum. Six mice were randomly assigned to receive irradiation, 16 Gy/1# to the heart base, and six were assigned to receive sham irradiation. Animals were closely monitored throughout the experiment and weighed at least twice per week to ensure <15% weight loss. All experimental procedures were carried out in accordance with the Home Office Guidance on the Operation of the Animals (Scientific Procedures) Act 1986, published by His Majesty's Stationery Office London, and were approved by the institutional Animal Welfare and Ethical Review Body (PPL2813).

Irradiation procedures

Animals were anesthetized with ketamine (100 mg/kg) and xylazine (10 mg/kg) by intraperitoneal injection before irradiation. Animals were irradiated with 220 kV x-rays at a dose rate of 2.67 Gy/min on a small-animal radiation research platform (Xstrahl Life Sciences, UK) calibrated using the Institute of Physics and Engineering in Medicine and Biology code of practice.[20] The cranial third of the heart was localized on cone beam computed tomography and a parallel, opposed, anterior-posterior field arrangement was created using a 3 × 9 mm collimator. Representative field arrangements from Muriplan are shown in Figure 1A-C.

Echocardiography

Transthoracic echocardiography (TTE) was performed at baseline and at 30 weeks after irradiation to assess structural and functional cardiac parameters using a Vevo770 ultrasound system with a high-frequency 45 MHz RMV707B scan head (VisualSonics Inc). Animals were anesthetized using 2% isoflurane during acquisition. Left ventricular metrics during systole and diastole were recorded for 2 seconds and 3 measurements were recorded during this window for each value. Using M-mode, the left ventricular ejection fraction (LVEF) and fractional shortening (LVFS) were derived from a parasternal short-axis view. Using pulse-wave Doppler imaging, E/A ratio, myocardial performance index

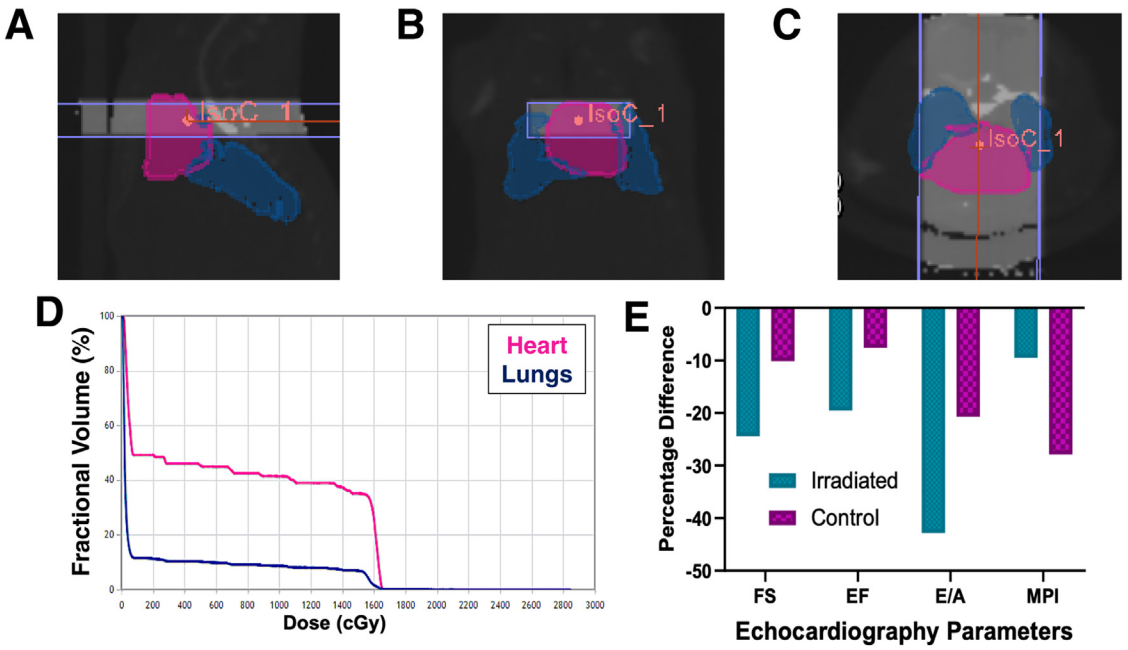

Fig. 1. Beam arrangement used for irradiations in the (A) sagittal, (B) coronal, and (C) transverse planes on cone-beam computed tomography. (D) The dose distribution in heart and lung are plotted in the dose volume histogram. (E) Functional cardiac parameters 30 weeks after 16 Gy radiation therapy to the heart base or sham irradiation.*Abbreviations:* E/A = E/A ratio, EF = left ventricular ejection fraction, FS = left ventricular fractional shortening, MPI = myocardial performance index.

(MPI) and isovolumetric relaxation times (IVRT) were calculated. Observers were blinded to the experimental groups of mice during data collection. Paired *t* tests were calculated for the functional parameters and histologic features. Pearson's correlation coefficient was generated for assessment of the relationship of DVH and TTE parameters.

Myocardial morphology

Tissue sections with atrial and ventricular tissue present were stained with hematoxylin (Dako Mayer's haematoxylin 10148347) and eosin (Sigma-Aldrich HT110216) (H&E), or Masson's trichrome (ab150686), as per manufacturer instructions. Pericardial thickness was evaluated on the former, and perivascular fibrosis on the latter, with 20 measurements made per section.

Spatial sample preparation and quality control

After the follow-up TTE, mice were humanely killed by cervical dislocation. Hearts were resected at the level of the ascending aorta and briefly rinsed in phosphate buffered saline to remove blood. The hearts of one irradiated and one control animal were embedded in Optimal Cutting Temperature compound (CellPath, Powys, Wales, UK) and snap-frozen using an isopentane slurry in dry ice, oriented carefully in the superior-inferior and right-left axes. To assess the RNA integrity number (RIN), 3, 10-μm cryosections of cardiac tissue were placed in RLT buffer (Qiagen, 1053393) and homogenized with a Precelleys lysing kit, CK28-R (P000916-LYSKo-A) using a Precelleys 24 tissue homogeniser (Bertin Technologies). Total RNA was extracted using an AllPrep DNA/RNA/miRNA Universal Kit (QIAGEN, 80224), according to the manufacturer's instructions. RIN was assessed using a 2100 Bioanalyzer (Agilent), with a threshold of 7.0 set for proceeding with spatial experiments. Additional sections for hematoxylin and eosin (H&E) staining were taken to check tissue morphology and for freeze artefacts.

Both hearts were cryosectioned at 10-μm thickness in the coronal plane. Consecutive tissue sections, each containing all 4 heart chambers and the great vessels, were placed within one of the slide capture areas (6.5 × 6.5 mm) of a chilled Visium Tissue Optimisation Slide (Visium Kit PN-1000191) and 2 Visium Spatial Gene GE Slides (Visium Kit PN-1000185) and stored at −80°C. Sections were stained with H&E, mounted in glycerol and brightfield images were taken on a Nikon A1R invert confocal microscope with a 10X objective.

Tissue optimization

The tissue optimization slide was used to determine permeabilization conditions for the heart tissue following the manufacturer's protocol. A permeabilization time of 40 minutes showed the optimum fluorescent cDNA signal and was used for the subsequent GE assays.

Gene expression

After tissue permeabilization and reverse transcription of the RNA captured by the GE slide, the probes were cleaved

from the slide and sequencing libraries prepared according to the manufacturer's protocol. Each GE slide capture area has ~5000 GE spots and the RNA captured by these probes share a common DNA barcode within the capture probe sequence that is used to spatially map the transcripts back to the tissue section, using the H&E images as reference. Each spot is 55 μm wide (resolution 1-10 cells) and these are separated by 45 μm. The cDNA was sequenced at 50,000 reads per spot using an Illumina NovaSeq 6000 and the resulting data aligned to reference genome (mm 10-3.0.0) using Space Ranger version 1.0.

Data quality and filtering

The count matrix was first enriched for protein-coding RNA and lincRNA gene types. Next, the expression matrix was filtered by removing *MALAT1* and *MTRNR* genes, as well as highly expressed genes related to hemoglobin. Spots with fewer than 500 genes and genes expressed in fewer than 15 spots were excluded. Spots with more than 10% mitochondrial GE were also discarded.

Sequence Alignment and Data Processing

The *Spaniel* package (v1.2.0, bioRxiv 619197) was used to import the data into R and to create the spot plot images. Normalization, dimensionality reduction, and integration of data from the 4 technical replicates for each heart were performed using the *Seurat* package (v3.1.3)[21] with a scale factor defined as the average of column sums across the expression matrix, using the *LogNormalize* method. Genes with high dispersion were selected using the *FindVariableGenes* function. Sources of technical and biological variability within the data, including cell cycle activity[22] and number of genes and mitochondrial content were regressed out using the *ScaleData* function. Spot plot images were generated for a prespecified list of genes from the literature to confirm visualized GE changes were appropriate.

Cluster visualization

Clusters were then identified using the *FindClusters* function. We used Uniform Manifold Approximation and Projection (UMAP) to visualize clusters in a reduced 2-D space. To identify differential GE within the clusters for each sample, pair-wise comparisons of individual clusters against all other clusters in the same sample were performed using the FindAllMarkers function in the Seurat package (version 3.1.3).[21] Clusters were visualized and their characteristics extracted using the 10X Loupe browser program. Human cardiac cell GE atlases were used to suggest likely cell populations.[23,24] The clusterProfiler package (version 3.16.1) was used to generate summary gene ontology (GO) dot plots for clusters with sufficient differential GE.

Subsequently, high-resolution bright field microscopy images were used to prospectively annotate histology corresponding to distinct heart regions on whole heart sections, namely the 4 chambers, great vessels, and valves (Fig. E1). A transverse strip of the superior ventricle was excluded from annotations to account for the uncertainty in the placement of the inferior border of the irradiation field for either or both animals. The bounds of this strip were decided based on anatomy (rather than pathology) by investigator group consensus, before analysis. GE data from all spot coordinates within labeled regions were averaged across spots permitting comparison of GE between the control and irradiated samples per annotated cardiac region.

Gene enrichment and network analysis

GO characteristics of genes from annotated substructures were determined using the ToppFun function of ToppGene[25] for all DE genes with an average $\log_{10}$ fold-change value >0.378 (corresponding to a fold-change of 1.3) and adjusted P value < .05. The entire set of genes identified across both samples was provided as a background gene list. The false discovery rate (Benjamini & Yekutieli) of <0.05 was taken to be significant for biological processes (BPs), and redundancies in the biological process lists were removed using Revigo.[26] Protein-protein interaction network analysis was performed on enriched genes using Cytoscape.[27] To confirm appropriate GE distributions visually before the analysis proper, comparisons with both normal[28] and postirradiation[29,30] whole-heart transcriptome study results were undertaken.

Results

Base radiosensitivity model

As shown previously, 16 Gy delivered in 1 fraction to the cranial third of the heart caused functional effects at late time points. The dose distribution to the heart and lungs is depicted in Figure 1D. Perivascular fibrosis and pericardial thickness were both increased in the atrial region of the irradiated animals compared with controls, without a corresponding difference in the ventricles (Figs. E2-4). TTE measurements at 30 weeks revealed more marked reductions in LVFS, LVEF, and E/A ratio in the irradiated mouse, and a less reduced MPI (Fig. 1E), in keeping with the expected deterioration in cardiac function. This was in keeping with the trends observed in treatment groups (n = 6) as a whole, in which LVFS and LVEF were significantly reduced and MPI was nonsignificantly increased (Fig. E5). Taken together, these results are indicative of left ventricular systolic dysfunction.

Evaluation of spatial transcriptomics

A total of 3543 and 3712 individual spots detected tissue for the control (n = 1) and irradiated animals (n = 1) respectively. An average of 2623 genes per spot were generated from 13,733 raw reads from an average of 18,706 unique transcripts per spot. The similarity in GE levels was comparable between technical replicates for both hearts was high as determined by Pearson's correlation.

To visualize distinct tissues as defined by GE patterns, spots were clustered as shown in the UMAP plots in Figure 2A and 2C. Overlaying these data on histology, clusters grossly corresponded to distinct heart regions, as demonstrated in the spot plots (Figs. 2B, 2D). Targeted searches for hallmark genes for each of the of cardiac domains, based on a recent human atlas (Table E1) confirmed appropriate spatial distribution patterns of cardiac cell populations on coregistered H&E (representative examples from the sham-irradiated heart are shown in Fig. 3, and the irradiated heart, in Fig. E6).

Dot plots were generated to grossly compare the distinguishing BPs within each sample (Fig. 4). In the unirradiated control tissue, our data showed that processes related to cellular respiration, lipid metabolism and the electron transport chain were predominant in line with the function of working cardiomyocytes. In contrast, in the irradiated base tissue, the most prevalent BPs were immune-related. The significantly dysregulated gene ontology profiles had minimal overlap in the BPs represented, suggesting a profoundly distinct transcriptional profile exists postirradiation with 16 Gy. Clusters from the base and nonbase regions are represented in the control and irradiated samples.

To visually assess whether GE changes after irradiation were spatially defined appropriately, spot plot images were generated for a prespecified set of genes from previous transcriptomic publications in cardiac irradiation murine models (Fig. E7).[28] PPARα and Nrf2 spot plots confirmed DE changes after irradiation localized to the irradiated heart volume of the cardiac base, and were not present in the ventricles. In contrast, TGF-β was not consistently upregulated in any heart region.

Of note, although the extra cluster identified in the irradiated heart could be a product of the clustering process, it likely represents thymus tissue included in the heart specimen, given that key gene upregulation in this cluster includes *FASN* (important in adipocytes) and CD74 (macrophages). Because the thymus effaces the anterior heart it is commonly found in cardiac specimens.

Region-specific GE changes

To analyze how GE changes differ between regions after irradiation, GE was averaged across all spots in each region and compared between the irradiated sample and the control. The

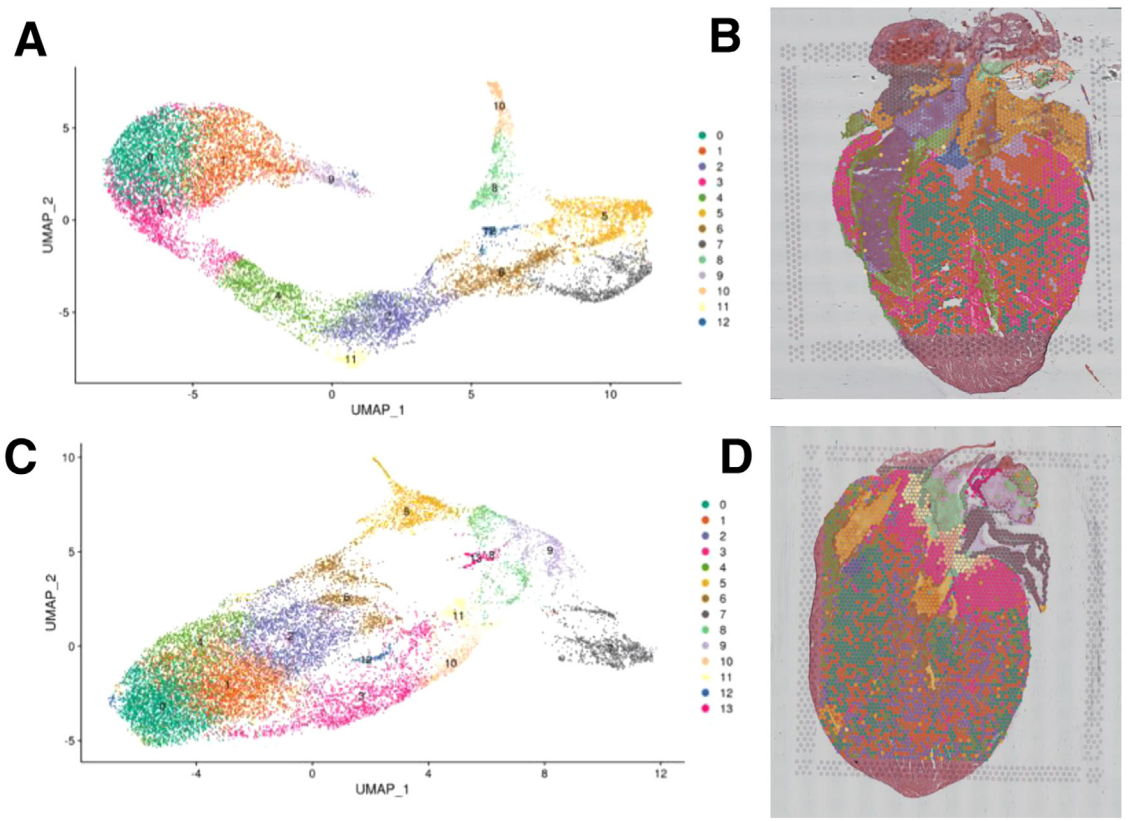

Fig. 2. On the left, integrated UMAP clusters for all 4 technical repeats for the (A) control and (C) irradiated heart. On the right, the corresponding spot plots generated to visualize the anatomic location of spots with different transcriptional profiles for (B) the control and (D) the irradiated heart.

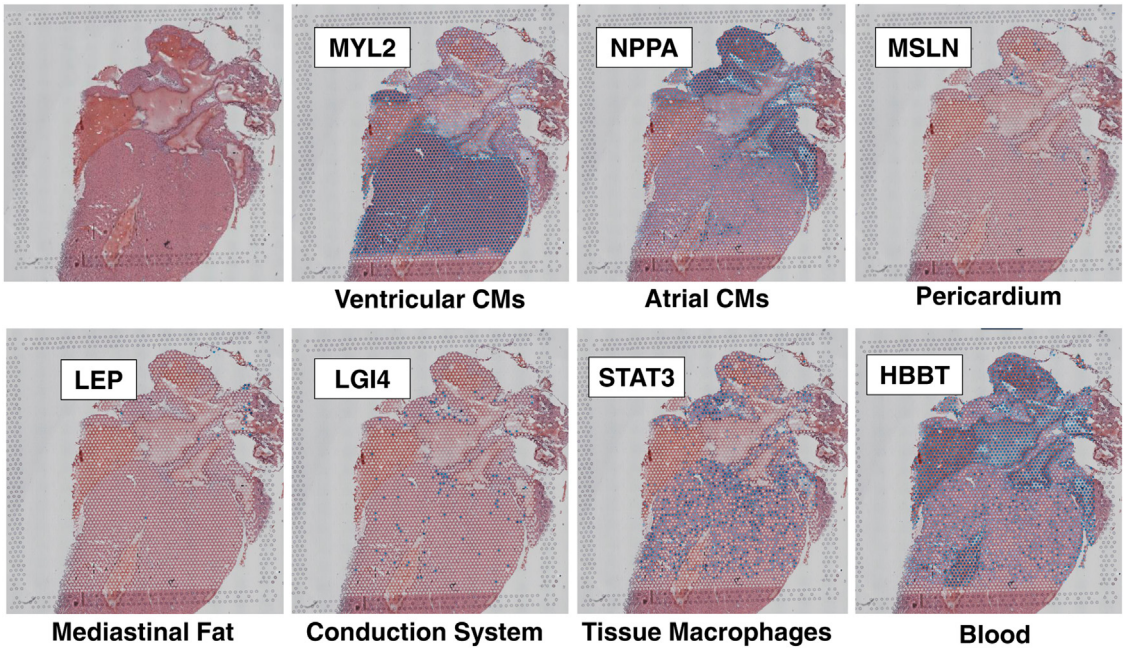

Fig. 3. Examples of spot visualization for upregulated genes representing key cardiac cell populations in the control heart. *Abbreviation*: CMs = cardiomyocytes.

significantly dysregulated GE predominantly localized to the volume of irradiated heart tissue (131 atrial genes vs 28 ventricular genes). Although genes were always dysregulated in the same direction between the right and left atria, less than a third were common to both regions, suggesting distinct and regional specific GE changes (Table E2).

In the right atrium of the irradiated case, the 3 most significantly activated BPs were extracellular matrix structure and organization, circulatory system development and regulation of cell population and proliferation (6%-8% genes in annotation). No BPs were significantly downregulated. The 5 most prominent nodal genes from a network analysis of all significantly dysregulated genes identified in the right atrium were *Fn1, Timp1, Cav1, Vwf* and *TagLn* (13°-26°), which are described in Table 1.

In contrast, in the left atrium, the 3 most significantly activated BPs were the classic complement pathway, B cell mediated immunity and response to interferon gamma (13%-50% genes in annotation). The most 3 most significantly downregulated BPs were regulation of calcium transmembrane transporter activity, regulation of heart contraction and cytokine-mediated pathways (6%-50% genes in annotation). The 5 most prominent nodal genes from a network analysis of all significantly dysregulated genes identified in the left atrium

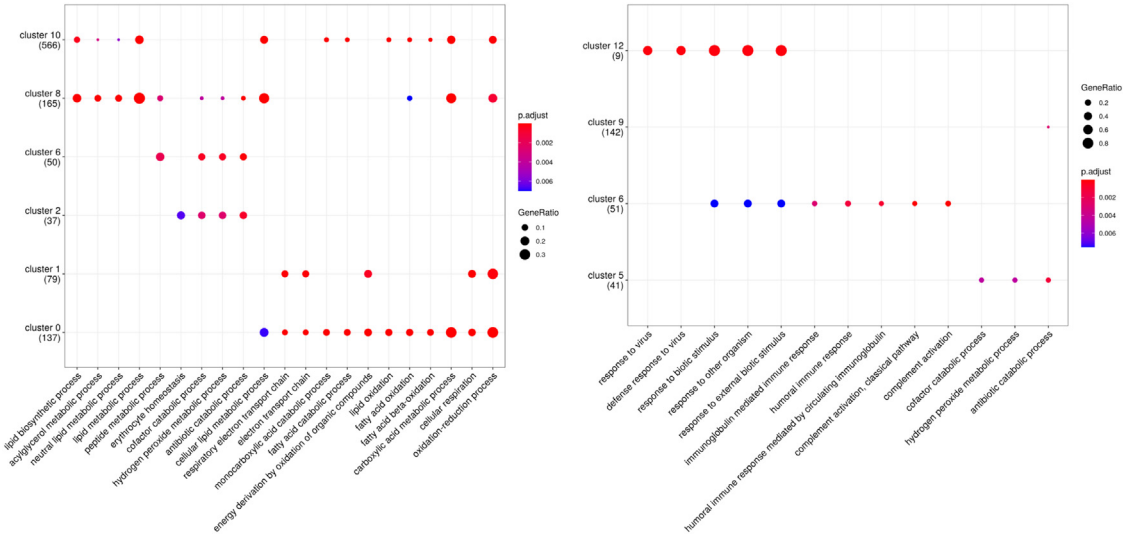

Fig. 4. Dot plots for the (A) unirradiated and (B) irradiated hearts. Clusters not represented did not show sufficient differentially expressed genes or were not significantly associated with a gene ontology term.

Table 1 Description of prominent nodal genes from network analysis of dysregulated atrial genes

Gene symbol	Gene name	Molecular function	Related biological processes	Laterality
Fn1	Fibronectin 1	Peptidase activator	Calcium-independent cell-matrix adhesion, cell-substrate junction assembly, and positive regulation of axon extension	Both
Timp1	Tissue inhibitor of metalloproteinase 1	Metalloendopeptidase inhibitor activity, cytokine activity, zinc binding activity	Connective tissue replacement involved in inflammatory response wound healing	Right
Cav1	Caveolin 1	Enzyme binding, identical protein binding, and protein heterodimerization	Blood vessel diameter maintenance, blood vessel morphogenesis, and negative regulation of signal transduction	Right
Vwf	Von Willebrand factor	Chaperone binding, identical protein binding, integrin binding activity	Platelet activation	Right
TagLn	Transgelin	Actin filament binding	Epithelial cell differentiation	Right
Myh6	Myosin heavy polypeptide 6, cardiac muscle α	Microfilament motor	Adult heart development, muscle cell development, regulation of heart contraction	Left
Col3a1	Collagen type III α1	SMAD binding	Aorta smooth muscle tissue morphogenesis, negative regulation of neuron migration, positive regulation of Rho protein signal transduction, cellular response to amino acid stimulus, collagen fibril organization	Left
C1qa	Complement component 1, q subcomponent α-polypeptide	Complement-mediated synapse pruning, microglial cell activation, nervous system development	Classical complement activation pathway	Left
Postn	Periostin, osteoblast-specific factor	Heparin binding activity	Cell adhesion, cellular response to vitamin K extracellular matrix organization, regulation of Notch signaling pathway, tissue development	Left

SMAD = SMA (small worm phenotype) and MAD (Mothers Against Decapentaplegic) gene families.

were *Fn1, Myh6, Col3a1, C1qa* and *Postn* (14°-28°) and are described in Table 3.[28] Spot plot images were generated for the key atrial genes for visualization (Fig. E8) illustrating how gene activation was generally restricted to the irradiated cardiac volume.

The majority (20 of 28) of the dysregulated ventricular genes were also dysregulated in the atria. Although the genes were always dysregulated in the same direction between the right and left ventricles, there was an insufficient number of significantly differentially expressed genes to generate GO BPs or network analyses for the individual ventricles. The 8 dysregulated genes unique to ventricular regions were *Hbb-bt, Ptgds, Myom2, Myh7, Ivns1abp, Lbh, Rpl13a,* and *Mlf1* which are described in Table E3.[28] The top 5 differentially expressed genes identified common to both the atria and ventricles were *Nppa, Myl7, Myl4, Malat1,* and *Sln,* and these genes are described in Table E4.[28]

Blood enters and leaves the heart via large vascular structures connected superiorly and are considered a part of the cardiac base. Although there were 39 significantly upregulated genes in the great vessels region, no significantly activated corresponding BPs were identified. The top 3 downregulated BPs were carboxylic acid metabolic process, ribose phosphate metabolic process, and organophosphate metabolic expression. The 5 most prominent nodal genes from a network analysis of all significantly dysregulated genes identified in the great vessels were *Sdha, Uqcrfs1, Uqcrc1, Atp5a1*, and *Cox4i1* (59°-64°), which are described in Table E5.[28]

The atrioventricular valves ensure unidirectional blood flow in the heart from atria to ventricles. From 259 upregulated genes in the valve region, the top 3 significant BPs were cell activation, immune effector process, and response to cytokine. From the 27 downregulated genes, the only significant downregulated biological process was muscle system process. The 5 most prominent nodal genes from a network analysis of all significantly dysregulated genes identified in the atrioventricular valves were *Actb, Gapdh, Fn1, CD44*, and *Tyrobp* (51°-106°), which are described in Table E6.[28]

The central region of the heart is a fibrous structure that plays an important structural role in the heart and includes the Bundle of His, which is the strands of the conduction system that coordinate ventricular contraction. From 362 upregulated genes in the central region, the top 3 significant BPs were extracellular matrix organization, extracellular structure organization, and external encapsulating structure organization. From the 404 downregulated genes, the top 3 significantly downregulated BPs were generation of precursor metabolites and energy, cellular respiration, and energy coupled proton transport down electrochemical gradient. The 5 most prominent nodal genes from a network analysis of all significantly dysregulated genes identified in the central region were *Il-1b, Itgb1, Acta2, Fn1,* and *Actb* (113°-195°), which are described in Table E7.[28]

Discussion

The heart is an elaborate organ that is classically described as being 'parallel' in terms of structure, yet several constituent substructures within the heart exhibit characteristics of serial tissue organization. These features suggest the potential for heterogeneity in underlying mechanisms of radiation response between the atria, ventricles and other important regions that are yet to be fully characterized. The base region, corresponding to the top of the heart, has been shown to mediate cardiac radiosensitivity in several clinical studies,[15-17] possibly due to the key substructures within, including the proximal coronary arteries and the conduction nodes. This region is particularly relevant in thoracic radiation therapy as primary lung and esophageal tumors and their regional nodal spread are typically within the immediate vicinity and therefore this cardiac region can get exposed to radical dose levels.

In this study, we present the first report of spatial GE in a translationally relevant model of cardiac toxicity after targeted irradiation of the heart base. Our murine model exhibits detectable cardiac dysfunction after 16 Gy image-guided radiation to the cranial third of the heart.[19] Unsupervised analysis enabled clusters of GE spots to be formed that represent distinct cardiac cell populations within the heart that spatially mapped to the corresponding H&E microanatomy. Gross comparison of the unsupervised dot plots for the 2 hearts enabled visualization of the most altered BPs per cluster that were predominantly related to immune and metabolic processes in the irradiated heart, in contrast to the control where a variety of normal physiological processes prevailed.

A direct comparison of gene profiles between regions of the heart was performed by annotation of H&E sections. Dysregulated GE was identified in all regions, with a 6-fold increase in the number of dysregulated genes in the atria compared with the ventricular regions suggesting that late GE changes predominantly localize to the irradiated heart volume yet changes in out-of-field cardiac regions were also observed. Considerable overlap was observed in the dysregulated genes of both atria and several genes were unique to both the atria and ventricular regions. Network analysis for each of the atrial regions revealed a distinct pattern of hub genes with only the *FN1* gene common to both regions.

The protein product of *FN1,* fibronectin 1, is a peptidase activator that maintains the extracellular matrix including calcium-independent cell-matrix adhesion, cell substrate junction assembly, and positive regulation of axon extension.[24] The tissue levels of fibronectin 1 are known to increase at 12 weeks after whole-heart irradiation with 21 Gy/7# in rats and are a known downstream mediator of TGF-β signaling, which has previously been implicated in normal tissue toxicity.[31] Differences in GE between right and left regions agrees with previous reports showing that laterality influences GE in healthy and diseased hearts.[32-34] Also, we identified other extracellular matrix-related genes in the network analysis of the atria including *Timp1, Col3a1,* and *Postn.*

Other pathways involved in the atria included the *Cav1, Tagln, Myh6* and *C1qa* genes suggesting the involvement of the vasculature, myocytes and complement pathways. These genes have also previously been implicated in the BPs mediating radiation toxicity in the heart.[35,36] or other normal tissues.[37] Of note, from the biological processes analysis, the upregulation of "hydrogen peroxide metabolic process," possibly related to previous oxidative stress resulting from targeted radiation, supports the mechanism by which antioxidant therapy may ameliorate RC (eg, vitamin E).[38]

A total of 28 genes were significantly up- or downregulated after 30 weeks in the ventricles, 8 of which were altered in the ventricles exclusively. Nodal genes from the network analysis of the protein products of these genes related to pathologic isoforms of myosin (*Myh7*), a key myocyte protein, and endocrine elements such as atrial natriuretic peptide (*NPPA*) and prostaglandin D2 synthase (*Ptgds*) that have been implicated in nonradiation disease states.[39] Upregulation of these genes may account for some elements of radiopathology previously described such as cardiomyocyte hypertrophy[35,40] and additional natriuretic peptide expression.[41]

Also, nonmuscular regions of the heart such as the valves and the great vessels each had unique patterns of GE postirradiation and key genes were related to regional functions (eg, integrin receptor beta, involved in collagen binding, in the central fibrous body which plays a skeletal role in the heart, and mitochondrial proteins in the great vessels, possibly linked to vascular smooth muscle).

As summarized in Figure 5, these novel data obtained through spatial transcriptomics offer insight into the underlying basis of regional radiation response in the heart. The genes identified as uniquely dysregulated in the atria require mechanistic validation and may improve our understanding of base radiosensitivity that has been observed clinically. Genes identified as distinctly dysregulated in the ventricular region are likely to play a role in how irradiation of the cardiac base affects other regions of the heart. Furthermore, cardiovascular drug screens with these molecular targets could help select cardiovascular drugs for future therapy studies for radiation cardiotoxicity prophylaxis.

Although regional heterogeneity in the GE patterns of the normal heart has been previously reported,[42] the

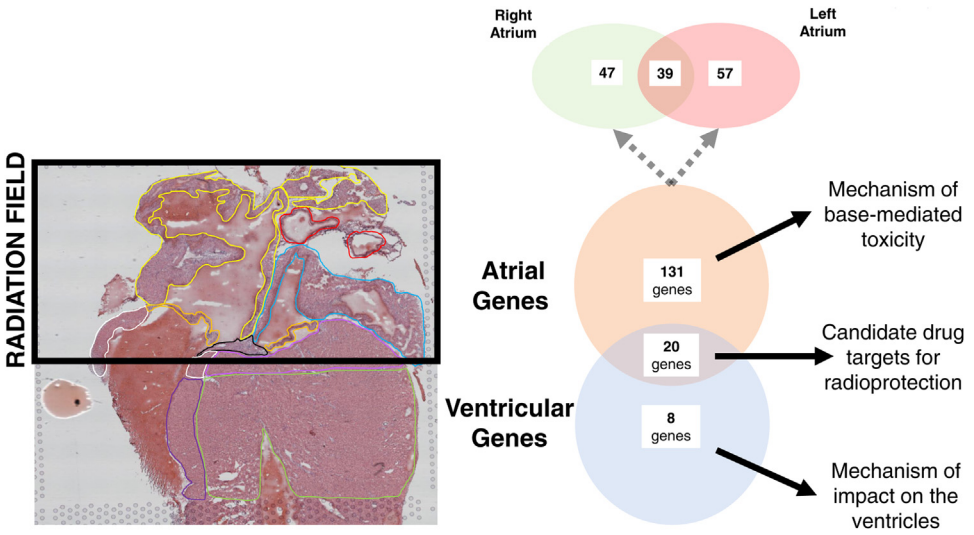

Fig. 5. Proposed schema for interpretation of partial heart irradiation spatial transcriptomic analyses. (Radiation field = black rectangle; right atrium = yellow; left atrium = blue; great vessels = red; right ventricle = purple; left ventricle = green; atrioventricular valves = orange; central fibrous body = black; irradiated right ventricle = white; irradiated left ventricle = pink.)

high-resolution tissue landscape has not been reported in the context of radiation response. A previous study identified >5000 differentially expressed genes in the rat left ventricles 1 week after whole-heart irradiation, showing that mitochondrial dysfunction, protein ubiquination, and sirtuin signaling were predominantly enriched.[43] The authors also showed that the oxidative stress modulating transcription factor *Nrf2* is involved as an important upstream regulator of the early radiation response, and *Nrf2* was shown to be upregulated in our study after cardiac base irradiation. *Nrf2* is a transcription factor for >1000 genes, and because many have been implicated in heart failure, it is subject to intense investigation at present.[44] Other similar studies combining transcriptomics and proteomics[30] highlight pathology relating to cardiac remodeling, metabolic perturbation, and fibrosis, which each have well-established positions in the etiology of RC.[40,45] Specifically, induction of the TGF-β pathway and inactivation of the PPAR-α pathway were shown, with evidence of cross-talk between the signaling via MAPK activation resulting from radiation. Our study found that PPAR-α is activated after cardiac base irradiation yet TGF-β was not upregulated in the spatial transcriptome, possibly because of the shorter follow-up and the reduced heart volume irradiated in our study.

In comparison with previous methods involving tissue microdissection or in situ sequencing, spatial transcriptomics allows for high-resolution, unbiased analysis of the transcriptional landscape.[46] This approach has been applied previously to resolve spatial heterogeneity in heart failure using cardiac biopsies,[47] to map embryonic cardiogenesis,[23] and to identify cellular differentiation and morphogenesis processes.[48] This study is the first spatial transcriptomic analysis of irradiated tissues and reveals distinct regional GE changes. Given the complex range of cell types in the heart, future studies may integrate single-cell sequencing with spatial transcriptomics, potentially using cardiac biopsies from patients undergoing radiation therapy to model clinically relevant baseline disease states such as ischemic heart disease or arrhythmia.

Although our study provides a robust analysis of the heterogeneous GE profile of the regional heart tissues, it has several limitations. Only 4 technical repeats were used from 2 animals and so individual, sample-specific variation may be important. In addition, the genes highlighted in the results were not independently examined by in situ hybridization or immunohistochemistry for additional validation, and this is recommended before such work is translated to a clinical context. Also, our analysis was performed at a single dose fractionation and time point, which may restrict extrapolation to the clinical scenario despite a similar biologically effective dose for typical lung cancer radiation treatment plans.[49] Despite these limitations, for the first time, we have demonstrated the application of spatial transcriptomics to provide unique, spatially resolved variations in GE in irradiated tissues. We anticipate that similar approaches will be increasingly implemented to better understand the spatial and temporal complexity of RT response in tumor and normal tissues.

Conclusion

We provide the first evidence of spatially resolved GE in a clinically relevant mouse model of RC. Our data give mechanistic insight into primary atrial and secondary ventricular radiation effects in the heart, advancing our understanding of regional variations in radiosensitivity. Furthermore, the novel approach employed is equally applicable to the study of radiation toxicities in other complex organs at risk to

refine the underlying mechanisms of tissue-specific radiation effects.

References

1. Atkins KM, Bitterman DS, Chaunzwa TL, et al. Mean heart dose is an inadequate surrogate for left anterior descending coronary artery dose and the risk of major adverse cardiac events in lung cancer radiation therapy. *Int J Radiat Oncol Biol Phys* 2021;110:1473-1479.
2. van Velzen SGM, Bruns S, Wolterink JM, et al. AI-based quantification of planned radiation therapy dose to cardiac structures and coronary arteries in patients with breast cancer. *Int J Radiat Oncol Biol Phys* 2022;112:611-620.
3. Xu C, Guo L, Liao Z, et al. Heart and lung doses are independent predictors of overall survival in esophageal cancer after chemoradiotherapy. *Clin Transl Radiat Oncol* 2019;17:17-23.
4. Milgrom SA, Bakst RL, Campbell BA. Clinical outcomes confirm conjecture: Modern radiation therapy reduces the risk of late toxicity in survivors of Hodgkin lymphoma. *Int J Radiat Oncol Biol Phys* 2021;111:841-850.
5. Darby SC, Cutter DJ, Boerma M, et al. Radiation-related heart disease: Current knowledge and future prospects. *Int J Radiat Oncol Biol Phys* 2010;76:656-665.
6. Mitchell JD, Cehic DA, Morgia M, et al. Cardiovascular manifestations from therapeutic radiation. *JACC CardioOncol* 2021;3:360-380.
7. Von Roeder M, Rommel KP, Kowallick JT, et al. Influence of left atrial function on exercise capacity and left ventricular function in patients with heart failure and preserved ejection fraction. *Circ Cardiovasc Imaging* 2017;10:e005467.
8. Bhar-Amato J, Davies W, Agarwal S. Ventricular arrhythmia after acute myocardial infarction: "The perfect storm. *Arrhythmia Electrophysiol Rev* 2017;6:134-139.
9. Di Bella G, Imazio M, Bogaert J, et al. Clinical value and prognostic impact of pericardial involvement in acute myocarditis: Data from the ITAMY. *Circ Cardiovasc Imaging* 2019;12:e008504.
10. Figueras J, Barrabés JA, Serra V, et al. Hospital outcome of moderate to severe pericardial effusion complicating ST-elevation acute myocardial infarction. *Circulation* 2010;122:1902-1909.
11. Baumgartner H, Falk V, Bax JJ, et al. 2017 ESC/EACTS guidelines for the management of valvular heart disease. *Eur Heart J* 2017;38:2739-2791.
12. Little WC, Freeman GL. Pericardial disease. *Circulation* 2006;113:1622-1632.
13. Walls GM, Lyon AR, Harbinson MT, Hanna GG. Cardiotoxicity following cancer treatment. *Ulster Med J* 2017;86:3-9.
14. Brown S, Banfill K, Aznaar M, Whitehurst P, Faivre Finn C. The evolving role of radiotherapy in non-small cell lung cancer. *Br J Radiol* 2019;92 110420190524.
15. McWilliam A, Kennedy J, Hodgson C, Vasquez E, Faivre-Finn C, van Herk M. Radiation dose to heart base linked with poorer survival in lung cancer patients. *Eur J Cancer* 2017;85:106-113.
16. McWilliam A, Khalifa J, Vasquez Osorio E, et al. Novel methodology to investigate the effect of radiation dose to heart substructures on overall survival. *Int J Radiat Oncol Biol Phys* 2020;108:1073-1081.
17. McWilliam A, Dootson C, Graham L, Banfill K, Abravan A, van Herk M. Dose surface maps of the heart can identify regions associated with worse survival for lung cancer patients treated with radiotherapy. *Phys Imaging Radiat Oncol* 2020;15:46-51.
18. Glatstein E. The omega on alpha and beta. *Int J Radiat Oncol Biol Phys* 2011;81:319-320.
19. Ghita M, Gill EK, Walls GM, et al. Cardiac sub-volume targeting demonstrates regional radiosensitivity in the mouse heart. *Radiother Oncol* 2020;152:216-221.
20. Aukett RJ, Burns JE, Greener AG, et al. Addendum to the IPEMB code of practice for the determination of absorbed dose for x-rays below 300 kV generating potential (0.035 mm Al−4 mm Cu HVL). *Phys Med Biol* 2005;50:2739-2748.
21. Satija R, Farrell JA, Gennert D, Schier AF, Regev A. Spatial reconstruction of single-cell gene expression data. *Nat Biotechnol* 2015;33:495-502.
22. Kowalczyk MS, Tirosh I, Heckl D, et al. Single-cell RNA-seq reveals changes in cell cycle and differentiation programs upon aging of hematopoietic stem cells. *Genome Res* 2015;25:1860-1872.
23. Asp M, Giacomello S, Larsson L, et al. A spatiotemporal organ-wide gene expression and cell atlas of the developing human heart. *Cell* 2019;179:1647-1660.e19.
24. Litviňuková M, Talavera-López C, Maatz H, et al. Cells of the adult human heart. *Nature* 2020;588:466-472.
25. Chen J, Bardes EE, Aronow BJ, Jegga AG. ToppGene Suite for gene list enrichment analysis and candidate gene prioritization. *Nucleic Acids Res* 2009;37:W305-W311.
26. Supek F, Bošnjak M, Škunca N, Šmuc T. REVIGO summarizes and visualizes long lists of gene ontology terms. *PLoS One* 2011;6:e21800.
27. Shannon P, Markiel A, Ozier O, et al. Cytoscape: A software environment for integrated models of biomolecular interaction networks. *Genome Res* 2003;13:2498-2504.
28. Alliance of Genome Resources Consortium. The Alliance of Genome Resources: Building a modern data ecosystem for model organism databases. *Genetics* 2019;213:1189-1196.
29. Schlaak RA, Frei A, Schottstaedt AM, et al. Mapping genetic modifiers of radiation-induced cardiotoxicity to rat chromosome 3. *Am J Physiol Heart Circ Physiol* 2019;316:H1267-H1280.
30. Subramanian V, Seemann I, Merl-Pham J, et al. Role of TGF beta and PPAR alpha signaling pathways in radiation response of locally exposed heart: Integrated global transcriptomics and proteomics analysis. *J Proteome Res* 2017;16:307-318.
31. Zhang KY, He XY, Zhou Y, et al. Atorvastatin ameliorates radiation-induced cardiac fibrosis in rats. *Radiat Res* 2015;184:611-620.
32. Tabibiazar R, Wagner RA, Liao A, Quertermous T. Transcriptional profiling of the heart reveals chamber-specific gene expression patterns. *Circ Res* 2003;93:1193-1201.
33. Johnson EK, Matkovich SJ, Nerbonne JM. Regional differences in mRNA and lncRNA expression profiles in non-failing human atria and ventricles. *Sci Rep* 2018;8:13919.
34. Ellinghaus P, Scheubel RJ, Dobrev D, et al. Comparing the global mRNA expression profile of human atrial and ventricular myocardium with high-density oligonucleotide arrays. *J Thorac Cardiovasc Surg* 2005;129:1383-1390.
35. Monceau V, Llach A, Azria D, et al. Epac contributes to cardiac hypertrophy and amyloidosis induced by radiotherapy but not fibrosis. *Radiother Oncol* 2014;111:63-71.
36. Boerma M, Roberto KA, Hauer-Jensen M. Prevention and treatment of functional and structural radiation injury in the rat heart by pentoxifylline and alpha-tocopherol. *Int J Radiat Oncol Biol Phys* 2008;72:170-177.
37. Markarian M, Krattli RP, Baddour JD, et al. Glia-selective deletion of complement C1q prevents radiation-induced cognitive deficits and neuroinflammation. *Cancer Res* 2021;81:1732-1744.
38. Liu H, Xiong M, Xia YF, et al. Studies on pentoxifylline and tocopherol combination for radiation-induced heart disease in rats. *Int J Radiat Oncol Biol Phys* 2009;73:1552-1559.
39. Zhao XS, Gallardo TD, Lin L, Schageman JJ, Shohet RV. Transcriptional mapping and genomic analysis of the cardiac atria and ventricles. *Physiol Genomics* 2003;12:53-60.
40. Seemann I, Gabriels K, Visser NL, et al. Irradiation induced modest changes in murine cardiac function despite progressive structural damage to the myocardium and microvasculature. *Radiother Oncol* 2012;103:143-150.
41. Kruse JJCM, Strootman EG, Bart CI, Visser A, Leer JWH, Wondergem J. Radiation-induced changes in gene expression and distribution of atrial natriuretic peptide (ANP) in different anatomical regions of the rat heart. *Int J Radiat Biol* 2002;78:297-304.
42. Sharma S, Razeghi P, Shakir A, Keneson BJ, Clubb F, Taegtmeyer H. Regional heterogeneity in gene expression profiles: A transcript analysis in human and rat heart. *Cardiology* 2003;100:73-79.

43. Schlaak RA, Frei A, SenthilKumar G, et al. Differences in expression of mitochondrial complexes due to genetic variants may alter sensitivity to radiation-induced cardiac dysfunction. *Front Cardiovasc Med* 2020;7:23.
44. Zang H, Mathew RO, Cui T. The dark side of Nrf2 in the heart. *Front Physiol* 2020;11:722.
45. Gabriels K, Hoving S, Seemann I, et al. Local heart irradiation of ApoE-/- mice induces microvascular and endocardial damage and accelerates coronary atherosclerosis. *Radiother Oncol* 2012;105:358-364.
46. Method of the year: Spatially resolved transcriptomics. *Nat Methods* 2021;18:9-14.
47. Asp M, Salmén F, Ståhl PL, et al. Spatial detection of fetal marker genes expressed at low level in adult human heart tissue. *Sci Rep* 2017;7:12941.
48. Mantri M, Scuderi GJ, Abedini-Nassab R, et al. Spatiotemporal single-cell RNA sequencing of developing chicken hearts identifies interplay between cellular differentiation and morphogenesis. *Nat Commun* 2021;12:1771.
49. Ueki K, Matsuo Y, Takeda A, et al. Impact of local recurrence on cause-specific death after stereotactic body radiotherapy for early-stage non-small cell lung cancer: Dynamic prediction using landmark model. *Int J Radiat Oncol Biol Phys* 2022;112:1135-1143.